NASA TECHNICAL NOTE

NASA TN D-5220

C. 1

NASA TN D-5220

AN ANALYSIS OF TERRAIN BIAS ERROR IN PLANETARY RADAR ALTIMETERS

by Richard F. Harrington and William D. Stanley

Langley Research Center
Langley Station, Hampton, Va.

NATIONAL AERONAUTICS AND SPACE ADMINISTRATION • WASHINGTON, D. C. • MAY 1969

AN ANALYSIS OF TERRAIN BIAS ERROR IN PLANETARY RADAR ALTIMETERS

By Richard F. Harrington and William D. Stanley

Langley Research Center
Langley Station, Hampton, Va.

NATIONAL AERONAUTICS AND SPACE ADMINISTRATION

For sale by the Clearinghouse for Federal Scientific and Technical Information
Springfield, Virginia 22151 – CFSTI price $3.00

AN ANALYSIS OF TERRAIN BIAS ERROR IN PLANETARY RADAR ALTIMETERS

By Richard F. Harrington and William D. Stanley*
Langley Research Center

SUMMARY

Terrain bias error in a pulse-modulated radar altimeter with an omnidirectional antenna and a leading-edge range tracker has been analyzed for planetary applications. This error is a result of the pulse distortion arising from the surface characteristics of a planet. The distortion is due to increasingly longer path lengths at larger incidence angles and the variation of the radar cross section with incidence angle.

The backscatter function of D. O. Muhleman was used as the radar cross-section model. An impulse response was first derived as a basis for determining arbitrary pulse returns by linear system techniques. An ideal square pulse was assumed for the transmitted pulse, and a computer program was developed for generating pulse returns. An ideal bandwidth-limited receiver was then simulated on the computer and used to filter the pulse returns. The position of the received pulse leading edge was defined as the time of the 50-percent-amplitude point of the pulse.

In order to assess the measurable error resulting from the pulse returns, an ideal square pulse was used as an input to the receiver simulation program. The position of the leading edge of the ideal square pulse after filtering was compared with that calculated from the pulse return. The difference between the respective leading edges represents the terrain bias error due to pulse distortion. Computations were performed for various filter types, transmitted pulsewidths, and bandwidths with input data chosen to include the possible range of planetary surface conditions.

Results of this investigation indicated that terrain bias error varies only slightly with filter type and number of poles, is approximately constant for bandwidths greater than one-half the reciprocal of the pulsewidth but increases significantly as the bandwidth is decreased, and is directly proportional to pulsewidth.

*Associate Professor of Engineering, Old Dominion College, Norfolk, Virginia (Consultant at NASA Langley Research Center).

INTRODUCTION

Altitude measurements are required in many aerospace systems. Altitude information is employed in guidance and control systems, in the correlation of science measurements, and in the determination of the vehicle trajectory. One method of measuring the altitude, when the direction of the surface directly below the vehicle is unknown, is to employ a pulse-modulated radar altimeter with a broad beamwidth antenna. One drawback of this approach is that energy is reflected from other directions and is received by the broad beamwidth antenna. However, the first return or leading edge of the received pulse represents the shortest distance to the surface or altitude. Variations in altitude and in surface reflection characteristics distort the received pulse and produce an error in the position of the leading edge known as the terrain bias error (ref. 1).

Two major effects contribute to the pulse distortion. The first effect is associated with a nonzero antenna beamwidth in conjunction with the spherical surface geometry. Energy leaving the transmitter with increasing look angle from the normal will experience increasingly longer time delay and, thereby, a spreading effect is produced. This effect can be calculated precisely if minor variations in the surface smoothness are neglected.

The second effect is the variation of the average or mean radar cross section with increasing incidence angle from the surface normal. The variation in radar cross section is difficult to determine precisely for a given planetary body because of the statistical nature of the random scatterers and the difficulty of obtaining measurements from remote planets. Several mathematical models have been proposed to describe the radar cross section of the planetary surfaces (refs. 2 to 5). Although many of these models have been found to yield satisfactory results, the Muhleman model (ref. 2) has been used to determine the radar cross-section model for both the Surveyor and Apollo lunar module programs. Radar cross-section measurements during lunar landing of the Surveyor showed good agreement with calculations made with the Muhleman model (ref. 6). Therefore, the Muhleman model was used in this investigation to compute the received pulse distortion due to variation in radar cross section with increasing incidence angle.

The purpose of this investigation was to analyze the terrain bias error in a pulse-modulated radar altimeter with an omnidirectional antenna. The radar cross-section model of Muhleman (ref. 2) was used as a basis for determining the radar returns due to an ideal transmitted pulse. The distorted received pulses were computed for both variations in altitude and surface reflection characteristics. The effect of filtering the distorted received pulses in a bandwidth-limited receiver was determined along with the effect of filtering an ideal undistorted received pulse. The position of the leading edge of the received pulse was defined as the time at which the leading edge had obtained an amplitude equal to 50 percent of its maximum amplitude. The terrain bias error,

determined by computing the additional time delay of the distorted pulses over the undistorted pulse, was obtained for different filter types, filter bandwidths, and transmitted pulsewidths.

SYMBOLS

For simplicity, the letters f and g have not been modified when expressed as functions of time. For example, the quantities f(t) and g(t) are obtained by replacing the angles θ and ϕ, respectively, by their appropriate functions of time. The same convention applies when the time scale is normalized for f, g, P, S, and y.

A	area, feet^2 (meters^2)
a	ratio of radar altitude to radius of planet
B	bandwidth of bandpass filter, hertz
c	speed of light, 9.836×10^8 feet/second (2.998×10^8 meters/second)
$f(\theta)$	normalized Muhleman backscatter function expressed in terms of incidence angle
f(t)	function obtained from $f(\theta)$ when θ is related to time
f(v)	function obtained from f(t) by normalizing the time scale
G	absolute antenna gain
G_o	maximum antenna gain
$g(\phi)$	normalized antenna gain function
g(t)	function obtained from $g(\phi)$ when ϕ is related to time
g(v)	function obtained from g(t) by normalizing the time scale
H	radar altitude, feet (meters)
K	amplitude factor for pulse echo

k	order of low-pass equivalent filter
n	index for computer samples
P_t	transmitted power, watts
P_r	received power, watts
$P(t)$	received signal resulting from transmitted impulse response
$P(v)$	received signal obtained from $P(t)$ by normalizing the time scale
R	radius of planet, feet (meters)
r	distance between radar and arbitrary point on surface, feet (meters)
$S(t)$	received signal resulting from transmitted step function
T	two-way time delay between radar and closest point on surface, seconds
t	time, seconds
t_p	transmitted pulsewidth, seconds
t_s	time between computer samples, seconds
v	normalized time variable
x	distance in excess of H between radar and planet along arbitrary ray, feet (meters)
$x(t)$	transmitted time function
$y(t)$	received time function before filtering
z	z-transform variable used in computer simulation
α	Muhleman coefficient
$\delta(t)$	impulse function

λ	wavelength, centimeters
σ	radar cross section, feet^2 (meters^2)
σ_o	radar backscatter function
$\hat{\sigma}_o$	value of σ_o at normal incidence
γ	planetary angle, degrees
ϕ	look angle, degrees
θ	incidence angle, degrees
τ	dummy time variable

DERIVATION OF TERRAIN BIAS ERROR

For the purpose of this investigation, a mathematical model of the radar cross section as a function of incidence angle was required. Earth based radar measurements of the Moon and planets have been used to determine models of the radar cross section. However, due to the close proximity of a radar altimeter to a planetary surface, the geometry used in analyzing its behavior must be different from the geometry employed in developing the model from Earth based measurements. The geometry of the altimeter problem is shown in figure 1. Models for the radar cross section have been developed as functions of the incidence angle θ. The initial portion of the pulse return is due to reflections from the area immediately below the spacecraft. In this region, θ is very small. Other portions of the pulse return are due to reflections from surface areas with larger incidence angles. The incidence angle may be uniquely related to the delay time for a given pulse return. Models of the angular dependence of the backscatter function may be derived from these data. This procedure as used with Earth based measurements is reviewed by Evans (ref. 4).

The fundamental radar equation is derived in such texts as Skolnik (ref. 7) and Barton (ref. 8). The radar equation relates the received power P_r to the transmitted power P_t by

$$P_r = \frac{P_t G^2 \lambda^2 \sigma}{(4\pi)^3 r^4} \tag{1}$$

where G is the absolute antenna gain, λ is the wavelength, σ is the radar cross section of the target, and r is the distance between target and radar. The radar cross section is related to the actual area A by

$$\sigma = \sigma_o A \tag{2}$$

where σ_o is the dimensionless backscatter factor (effective area per unit actual area).

The preceding relationships are adequate for small targets, but they require modification for analyzing the exact behavior of a widely dispersed target such as that encountered in a radar altimeter. A differential contribution of received power dP_r due to a differential cross section $d\sigma$ may be expressed as

$$dP_r = \frac{P_t G^2 \lambda^2 \, d\sigma}{(4\pi)^3 r^4} \tag{3}$$

The quantity $d\sigma$ may be related to a differential section of surface area by

$$d\sigma = \sigma_o \, dA \tag{4}$$

The backscatter function σ_o is, in general, a function of the incidence angle.

Muhleman (ref. 2) derived a model of the radar backscatter function for a planetary surface based on geometric optics and statistical theory. The relationship developed by Muhleman contains a single parameter α, which is a function of both the planet roughness and the radar frequency. The model developed by Muhleman is expressed as

$$\sigma_o = \frac{\hat{\sigma}_o \alpha^3 \cos \theta}{(\sin \theta + \alpha \cos \theta)^3} \tag{5}$$

where $\hat{\sigma}_o$ is the value of σ_o at normal incidence ($\theta = 0^o$). The quantity α is the Muhleman coefficient, which represents the effective mean slope of the planet surface. The exact variation of α with frequency is not known. However, it has been determined (ref. 2) that for the lunar surface α increases with frequency. The value of α is lower for a smoother, more specular surface and is greater for a rougher, more diffuse surface. Typical values obtained by Muhleman (ref. 2) are $\alpha = 0.265$ for the Moon and $\alpha = 0.1$ for Venus, both values being obtained at $\lambda = 12.5$ cm.

Equation (5) may be written in the form

$$\sigma_o = \hat{\sigma}_o f(\theta) \tag{6}$$

where $f(\theta)$ may be defined as the normalized backscatter function. (Note that $f(0^o) = 1$.) Insertion of equations (4), (5), and (6) into equation (3) results in

$$dP_r = \frac{P_t G^2 \lambda^2 \hat{\sigma}_o f(\theta) \, dA}{(4\pi)^3 r^4} \tag{7}$$

A very convenient means for characterizing a solution of this equation is by using the impulse response. The general form of the received power function $P(t)$ due to an impulse excitation is derived in appendix A. The function obtained is

$$P(t) = \frac{K}{T} \frac{g^2(t)f(t)}{\left(1 + \frac{t}{T}\right)^3} \tag{8}$$

where K is a constant defined by equation (A23) and T is the two-way delay time along the shortest path as defined by equation (A11). The quantities $g(t)$ and $f(t)$ represent, respectively, the normalized antenna gain function and the normalized Muhleman backscatter function, both expressed as functions of the two-way time required for a particular component of the signal to reach the antenna. The time $t = 0$ is chosen at the beginning of the return echo.

The Muhleman backscatter function expressed in terms of time is developed in appendix B. In order to simplify some rather unwieldy expressions, the approximation $t << T$ was made. This approximation is quite good for most of the cases analyzed. With this assumption, the approximate impulse response is given by

$$P(t) = \frac{K}{T} \frac{\alpha^3 g^2(t)}{\left(1 + \frac{t}{T}\right)\left[\alpha + \left(1 + \frac{a}{2}\right)\left(1 + \frac{t}{4T}\right)\sqrt{\frac{2t}{T}}\right]^3} \tag{9}$$

The antenna gain must be related to time and placed in equation (9) before the response due to an arbitrary pulse excitation may be determined.

In general, the return echo due to any arbitrary transmitted pulse can be determined by convolving the transmitted pulse $x(t)$ with the impulse response $P(t)$. For the purpose of this investigation, an ideal square pulse was assumed for $x(t)$. With the ideal square pulse, it is not necessary to perform a complete convolution. Instead, the step response may be determined as a basis for representing the pulse response. The step response $S(t)$ is related to the impulse response $P(t)$ by

$$S(t) = \int_0^t P(t)\, dt \tag{10}$$

It is shown in appendix C that for an omnidirectional antenna and with the approximation $t << T$, the step response is

$$S(t) = \frac{K\alpha^2}{\left(1 + \frac{a}{2}\right)^2}\left\{\frac{1}{2} - \frac{1}{1 + \left(1 + \frac{a}{2}\right)\frac{\sqrt{\frac{2t}{T}}}{\alpha}} + \frac{1}{2\left[1 + \left(1 + \frac{a}{2}\right)\frac{\sqrt{\frac{2t}{T}}}{\alpha}\right]^2}\right\} \tag{11}$$

Let t_p represent the pulsewidth of the ideal square pulse and $y(t)$ represent the received signal. The received signal may be expressed as

$$y(t) = S(t) \qquad (0 < t < t_p)$$

$$y(t) = S(t) - S(t - t_p) \qquad (t > t_p) \qquad (12)$$

It should be emphasized that $y(t)$ is not the actual RF received signal, but rather it is the video (envelope) representation of the signal when a perfect square law detector is employed. At the receiver, it is necessary to filter the received signal $y(t)$ with a low-pass filter to improve the signal-to-noise ratio. The details of the computer filter simulation employed in this investigation are outlined in appendix D.

Although a pulse return is already distorted when it arrives at the receiver, the filter introduces further distortion and time delay. The total delay of a pulse may be defined as the time measured to the 50-percent-amplitude point of the pulse. As a means of assessing the time delay resulting from the terrain bias, an ideal square pulse may be compared with the distorted pulse return. If both pulses are processed through a filter, the difference in time delay of the two signals is a measure of the time delay error due to terrain bias. Thus, terrain bias error is defined as the difference in time delay, after filtering, between a perfect undistorted pulse and the actual distorted pulse return.

RESULTS AND DISCUSSION

The parameters that were employed in the investigation of terrain bias error are presented in table 1.

TABLE 1.- DEFINITION OF PARAMETERS

Variable	Symbol	Unit	Values
Transmitted pulsewidth	t_p	μsec	0.1, 1.0, 10
Surface specularity	α		0.01, 0.1, 1.0
Altitude	H	feet	10^3, 5×10^3, 5×10^4, 5×10^5
		(meters)	(310), (1.53×10^3), (1.53×10^4), (1.53×10^5)
Bandwidth	B	Hertz	$0.1/t_p$, $0.3/t_p$, $0.5/t_p$, $5.0/t_p$

The rationale used in selection of the parameters was to cover values that might be employed in a pulse-modulated radar altimeter designed for planetary entry missions. The radius of Mars was used in the geometric relationships, and the altitude range of 1000 to 500 000 ft (310 to 153 000 m) was chosen to represent the range of interest for a Martian entry. However, this analysis can be used for any planet by proper scaling of

the altitude values by the ratio of planet radii. The values of α were selected to provide a broad range that includes the Moon, Mars, and Venus (refs. 2 and 5). A pulsewidth of 1 μsec is typical of this type of altimeter, and it was used for most of this investigation. Pulsewidths of 0.1 μsec and 10 μsec were also employed to study the effect of pulsewidth variation on the terrain bias error.

The optimum post-detection bandwidth for the receiver in a pulse-modulated radar altimeter is one-half the reciprocal of the pulsewidth (refs. 1, 7, and 8). The bandwidth was varied above and below this value to study the effects on the terrain bias error.

The filter characteristics considered in varying the bandwidth were those of the Butterworth (maximally flat-amplitude response), Chebyshev (3-dB ripple), and maximally flat-time-delay filters. These filter characteristics are probably the most common types encountered in modern radar systems. The differences between the frequency domain behavior of the three filters represent a wide variation of trade-off between magnitude and phase characteristics. The bandwidth is defined as the width in Hz between the appropriate 3-dB points. The number of poles for each filter was varied from one to four to study the effects of increasing stop-band attenuation. For the one-pole filter, all three filter types are identical. Thus, a total of 10 different filter responses were considered.

The pulse responses were computed for the different altitudes and surface specularities given in table 1. A pulsewidth of 1 μsec was selected for developing most of the data in this report. Only the relative amplitudes of the received pulses are presented; that is, the pulse amplitudes are normalized to unity maximum value. The pulse response would be typical of a video pulse which has been detected by a perfect square-law detector in an infinite bandwidth receiver. The normalized pulse responses are presented for various radar altitudes and values of Muhleman coefficient in figures 2 and 3, respectively. For $\alpha = 0.01$, the normalized pulse responses at the two lower altitudes are close replicas of the transmitted pulse (fig. 2(a)). For $\alpha = 0.1$, the responses at the two higher altitudes approach ramps during the rising portion of the pulse returns (fig. 2(b)). For $\alpha = 1.0$, most of the responses approximate ramps during the rising portion of the pulse returns (fig. 2(c)). By comparing figures 2(a), 2(b), and 2(c), it can be seen that increasing α by 1 decade corresponds closely to increasing the altitude by 2 decades, in terms of the normalized pulse shape.

The data for H = 5000 ft (1530 m), 50 000 ft (15 300 m), and 500 000 ft (153 000 m) from figure 2 are cross-plotted in figures 3(a), 3(b), and 3(c), respectively, to show the effect of α at several different altitudes.

The pulse responses shown in figures 2 and 3 assumed an infinite bandwidth receiver. Radar altimeters require a filter in the receiver to limit the noise input. However, these pulse responses are distorted by the use of a finite bandwidth filter. The results of filtering a 1-μsec pulse which has been reflected from a planet's surface with a specularity

of $\alpha = 0.1$ in a three-pole Butterworth filter are shown for different altitudes in figure 4(a). The amplitude of the filtered pulse is normalized to the maximum value of the nonfiltered pulse echo. Thus, the loss in pulse amplitude to filtering can be determined from figure 4(a). The nonfiltered pulse echo distortion for $\alpha = 0.1$ and a pulsewidth of 1 μsec is shown in figure 2(b). A comparison of figures 2(b) and 4(a) reveals that the varying pulse distortion with altitude prior to filtering results in a variation of time delay with altitude after filtering. This variation in time delay is one of the sources of the terrain bias error.

The relationship between pulse distortion due to variation in surface specularity and pulse distortion due to variation in altitude has previously been discussed and illustrated in figures 2 and 3. Therefore, a variation in surface specularity results in a similar variation of time delay of the filtered pulse response and contributes to the terrain bias error.

Similar normalized filtered pulse responses for the three-pole maximally flat-time-delay and three-pole Chebyshev (3-dB ripple) filters are shown in figures 4(b) and 4(c), respectively.

The terrain bias error was computed for a 1-μsec-wide pulse for surface specularities of $\alpha = 0.01$, 0.1, and 1.0 by using a three-pole Butterworth filter, a three-pole maximally flat-time-delay filter, and a three-pole Chebyshev (3-dB ripple) filter. The terrain bias error for a 1-μsec-wide pulse and a three-pole Butterworth filter with a bandwidth equal to one-half the reciprocal of the pulsewidth is shown in figure 5(a) as a function of altitude. Data for constant specularities of $\alpha = 0.01$, 0.1, and 1.0 are presented. Similarly, the terrain bias errors for a three-pole maximally flat-time-delay filter and a three-pole Chebyshev (3-dB ripple) filter are shown in figures 5(b) and 5(c), respectively.

Maximum absolute terrain bias error is largest at the highest altitude and for the most diffuse surface. A study was made to determine the effect of various filter characteristics on the terrain bias error under worst altitude and surface conditions (i.e., altitude of 500 000 ft (153 000 m) and a diffuse surface corresponding to $\alpha = 1.0$). The Butterworth, Chebyshev (3-dB ripple), and maximally flat-time-delay filters were used, and the number of filter poles was varied from one to four. The terrain bias error was calculated for each combination of filter type and number of filter poles. The terrain bias error averaged over all the filter and pole combinations considered was 252 ft (77 m). The maximum error was 269 ft (82 m) and the minimum error was 234 ft (71 m). From these results, it can be deduced that the terrain bias error varies only slightly with filter type and number of filter poles. Therefore, the choice of the filter type and number of filter poles would be made from other considerations such as receiver signal-to-noise performance, filter construction, and so forth.

The effect of variation in filter bandwidth and transmitted pulsewidth on the terrain bias error was also determined. The bandwidth of the filters was varied from $0.1/t_p$ to $5/t_p$. The maximum terrain bias error as a function of altitude is shown in figure 6 for a 1-μsec-wide pulse and a three-pole Butterworth filter. The error is essentially the same for bandwidths between $0.5/t_p$ and $5/t_p$ and increases for bandwidths less than $0.5/t_p$.

The maximum terrain bias error for a three-pole Butterworth filter with a bandwidth of $0.5/t_p$ is shown in figure 7 as a function of altitude for different pulsewidths. The terrain bias error is directly proportional to pulsewidth. Therefore, for a pulse-modulated radar altimeter with an omnidirectional antenna and a leading-edge range tracker, the pulsewidth determines terrain bias error for an optimum bandwidth and ultimately provides a limiting factor in the overall accuracy of the radar altimeter.

The maximum possible terrain bias error due to both variations in altitude and surface reflection characteristics is one-half the time delay equivalent to a pulse width. This error could be reduced significantly if the variation in altitude and/or the surface reflection characteristics were known.

CONCLUSIONS

Analysis of the terrain bias error of a pulse-modulated radar altimeter resulted in the following conclusions:

1. Terrain bias error is directly proportional to pulsewidth.

2. Terrain bias error is approximately constant for receiver post-detection filter bandwidths greater than one-half the reciprocal of the pulsewidth and increases significantly as the bandwidth is decreased.

3. Terrain bias error varies only slightly with filter type and number of filter poles.

4. The maximum terrain bias error due to both variations in altitude and surface reflection characteristics is approximately one-half the pulsewidth. This error could be reduced significantly if the surface reflection characteristics were known.

Langley Research Center,
National Aeronautics and Space Administration,
Langley Station, Hampton, Va., March 17, 1969,
125-22-02-16-23.

APPENDIX A

DERIVATION OF THE RADAR ECHO IMPULSE RESPONSE

A two-dimensional projection of the planetary-radar-altimeter model is shown in figure 1. The altitude H represents the distance of the spacecraft radar above the planetary surface, and x represents the additional one-way distance required for a particular component of the signal to travel. The angles ϕ, θ, and γ are, respectively, the look angle, the incidence angle, and the planetary angle.

Equation (7) in the main body of the report relates a differential element of power to the corresponding differential unit of area. The relationship is

$$dP_r = \frac{P_t G^2 \lambda^2 \hat{\sigma}_o f(\theta)\, dA}{(4\pi)^3 r^4} \tag{A1}$$

The differential unit of area dA may be related to the planetary angle γ (see fig. 1) by the following equation:

$$dA = 2\pi R^2 \sin\gamma\, d\gamma \tag{A2}$$

The distance r may be expressed as

$$r = H + x \tag{A3}$$

Insertion of equations (A2) and (A3) into equation (A1) yields

$$dP_r = \frac{P_t G^2 \lambda^2 \hat{\sigma}_o R^2 f(\theta) \sin\gamma\, d\gamma}{2(4\pi)^2 (H + x)^4} \tag{A4}$$

In general, the quantities x and G can be considered to be functions of either ϕ or γ. Let

$$G = G_o g(\phi) \tag{A5}$$

where G_o is the maximum antenna gain, and $g(\phi)$ is the normalized antenna gain function. Substitution of equation (A5) into equation (A4), and manipulation of the denominator yields

$$dP_r = \frac{G_o^2 \lambda^2 \hat{\sigma}_o R^2}{2(4\pi)^2 H^4} \frac{P_t g^2(\phi) f(\theta) \sin\gamma\, d\gamma}{\left(1 + \frac{x}{H}\right)^4} \tag{A6}$$

Now, let

$$K_1 = \frac{G_o^2 \lambda^2 \hat{\sigma}_o R^2}{2(4\pi)^2 H^4} \tag{A7}$$

Equation (A6) now becomes

$$dP_r = \frac{K_1 P_t g^2(\phi) f(\theta) \sin \gamma \, d\gamma}{\left(1 + \frac{x}{H}\right)^4} \tag{A8}$$

A fundamental means of characterizing the nature of the return echo is by using the impulse response. Assume then that P_t is a unit impulse – that is,

$$P_t = \delta(t) \tag{A9}$$

To utilize the impulse function, it is necessary to relate the differential $d\gamma$ to time. Application of the law of cosines yields the following relationship between x and γ (fig. 1):

$$\cos \gamma = 1 - \frac{x^2 + 2xH}{2\left(R^2 + RH\right)} \tag{A10}$$

Assume now that $t = 0$ is defined as the beginning of the leading edge of the return echo. Let T represent the two-way time delay of travel from the spacecraft to the planet along the shortest distance. This value is

$$T = \frac{2H}{c} \tag{A11}$$

where c is the speed of light. Let τ, a dummy variable representing the two-way time delay due to the distance x, be given by

$$\tau = \frac{2x}{c} \tag{A12}$$

and note that

$$\frac{\tau}{T} = \frac{x}{H} \tag{A13}$$

Manipulation of equation (A10) with the use of equations (A11), (A12), and (A13) yields

$$\cos \gamma = 1 - \frac{H^2\left[\left(\frac{\tau}{T}\right)^2 + 2\left(\frac{\tau}{T}\right)\right]}{2R^2\left(1 + \frac{H}{R}\right)} \tag{A14}$$

For convenience, let

$$a = \frac{H}{R} \tag{A15}$$

Use of equation (A15) in equation (A14) results in

$$\cos \gamma = 1 - \frac{a^2\left[\left(\frac{\tau}{T}\right)^2 + 2\left(\frac{\tau}{T}\right)\right]}{2(1 + a)} \tag{A16}$$

APPENDIX A

Differentiation of both sides of equation (A16) yields

$$\sin \gamma \, d\gamma = \frac{a^2\left(1 + \frac{\tau}{T}\right) d\tau}{T(1 + a)} \tag{A17}$$

Substitution of equation (A17) into equation (A8) results in

$$dP_r = \frac{a^2 K_1 P_t g^2(\tau) f(\tau) \, d\tau}{T(1 + a)\left(1 + \frac{\tau}{T}\right)^3} \tag{A18}$$

where $g(\phi)$ and $f(\theta)$ have been redefined in terms of τ. A contribution of received power at time t is due to power transmitted at time $t - \tau$. Since the entire time scale has been shifted, the received power $P(t)$ can be written as

$$P(t) = \frac{a^2 K_1}{T(1 + a)} \int_0^\infty \frac{g^2(\tau) f(\tau) \delta(t - \tau) \, d\tau}{\left(1 + \frac{\tau}{T}\right)^3} \tag{A19}$$

A fundamental definition of the impulse function is

$$\int_0^\infty h(\tau)\delta(t - \tau) \, d\tau = h(t) \tag{A20}$$

Application of equation (A20) to equation (A19) yields

$$P(t) = \frac{a^2 K_1}{T(1 + a)} \frac{g^2(t) f(t)}{\left(1 + \frac{t}{T}\right)^3} \tag{A21}$$

The constant factor may be modified. Let

$$K = \frac{a^2 K_1}{1 + a} \tag{A22}$$

Substitution of equations (A7) and (A15) into equation (A22) yields

$$K = \frac{G_o{}^2 \lambda^2 \hat{\sigma}_o}{2(4\pi)^2 (1 + a) H^2} \tag{A23}$$

Equation (A21) now becomes

$$P(t) = \frac{K}{T} \frac{g^2(t) f(t)}{\left(1 + \frac{t}{T}\right)^3} \tag{A24}$$

where the factor T has been retained separately for reasons that will be clear later. The function $P(t)$ is the radar echo impulse response. For reasons of convenience in

subsequent work, it is desirable to define a normalized time variable v. Let

$$v = \frac{t}{T} = \frac{x}{H} \tag{A25}$$

Substitution of equation (A25) into equation (A24) results in

$$P(v) = \frac{K}{T} \frac{g^2(v)f(v)}{(1 + v)^3} \tag{A26}$$

APPENDIX B

MUHLEMAN LAW APPROXIMATION

The basic form of the Muhleman equation is investigated, and certain simplifying approximations are made. The use of such approximations results in a simpler computational form for studying the pulse response.

The Muhleman backscatter function is given by

$$f(\theta) = \frac{\alpha^3 \cos\theta}{(\sin\theta + \alpha\cos\theta)^3} \tag{B1}$$

The angle θ must now be related to time if equation (B1) is to be employed in the application of equation (A24) or subsequent results. An application of the law of sines to the geometry of figure 1 results in

$$\sin\theta = \frac{1+a}{a\left(1+\frac{x}{H}\right)}\sin\gamma \tag{B2}$$

Substitution of the normalized time variable of equation (A25) into equation (B2) yields

$$\sin\theta = \frac{1+a}{a(1+v)}\sin\gamma \tag{B3}$$

The same substitution applied to equation (A16) yields

$$\cos\gamma = 1 - \frac{a^2(v^2+2v)}{2(1+a)} \tag{B4}$$

Simultaneous solution of equations (B3) and (B4) for $\sin\theta$ results in

$$\sin\theta = \frac{1}{v+1}\sqrt{v(v+2)\left[1+a-\frac{a^2v(v+2)}{4}\right]} \tag{B5}$$

Generally, almost all of the transmitted energy from an impulse-type excitation will be returned within a fraction of the time T measured from the leading edge of the pulse return. This condition implies that the normalized time v will be very small in the interval of primary interest; that is, $v \ll 1$. Furthermore, in the range of altitude measurements of interest, $a \leqq 1$. With these assumptions a careful analysis of equations (B4) and (B5) yields the following approximations:

$$\cos\theta \approx \frac{1}{1+v} \tag{B6}$$

APPENDIX B

$$\sin\theta \approx \frac{\left(1+\frac{a}{2}\right)\left(1+\frac{v}{4}\right)\sqrt{2v}}{1+v} \tag{B7}$$

Substitution of equations (B6) and (B7) into equation (B1) yields for the approximate Muhleman backscatter function

$$f(v) \approx \frac{(1+v)^2}{\left[1+\left(1+\frac{a}{2}\right)\left(1+\frac{v}{4}\right)\frac{\sqrt{2v}}{\alpha}\right]^3} \tag{B8}$$

Equation (B8) may now be substituted into equation (A26) to yield, for the impulse response,

$$P(v) \approx \frac{Kg^2(v)}{T(1+v)\left[1+\left(1+\frac{a}{2}\right)\left(1+\frac{v}{4}\right)\frac{\sqrt{2v}}{\alpha}\right]^3} \tag{B9}$$

APPENDIX C

DEVELOPMENT OF THE STEP RESPONSE

The radar echo impulse response was derived in appendix A and simplified in appendix B. In this appendix, the step response is developed from the impulse response. The step response may be used as a basis for determining the actual return from a transmitted square pulse as indicated by equation (11).

The step response $S(t)$ is related to the impulse response $P(t)$ by

$$S(t) = \int_0^t P(t)\, dt \tag{C1}$$

By substituting equations (A25) and (B9) into (C1), the step response becomes

$$S(v) = K \int_0^v \frac{g^2(v)\, dv}{(1 + v)\left[1 + \left(1 + \frac{a}{2}\right)\left(1 + \frac{v}{4}\right)\frac{\sqrt{2v}}{\alpha}\right]^3} \tag{C2}$$

Assume now that the antenna is omnidirectional – that is, $g(v) = 1$ – and that the region of primary interest is where $t \ll T$ or $v \ll 1$. A study of equation (C2) reveals that with these assumptions, the step response may be closely approximated by

$$S(v) \approx \frac{K}{1 + v} \int_0^v \frac{dv}{\left[1 + \left(1 + \frac{a}{2}\right)\frac{\sqrt{2v}}{\alpha}\right]^3} \tag{C3}$$

Although the evaluation of (C3) is not completely routine, the details are omitted since this operation may be deduced from standard integration procedures. The result is

$$S(v) = \frac{K\alpha^2}{(1 + v)\left(1 + \frac{a}{2}\right)^2}\left\{\frac{1}{2} - \frac{1}{\left[1 + \left(1 + \frac{a}{2}\right)\frac{\sqrt{2v}}{\alpha}\right]} + \frac{1}{2\left[1 + \left(1 + \frac{a}{2}\right)\frac{\sqrt{2v}}{\alpha}\right]^2}\right\} \tag{C4}$$

APPENDIX D

DIGITAL-COMPUTER FILTER SIMULATION

The process in which a continuous analog filter can be simulated by discrete numerical operations on a digital computer is a problem too involved and inappropriately related to the principal problem to warrant detailed consideration in this report. Among the sources dealing with the details of digital simulation are reference 9 by Kaiser and work performed by William D. Stanley at Goddard Space Flight Center while on NASA-ASEE Faculty Fellowship in August 1965. A brief discussion of the simulation is presented in this appendix.

The technique employed in the digital simulation was to use a standard linear transfer function in the p-plane and to map this function to the domain of sampled data system (z-plane) by means of the bilinear transformation. This transformation reads

$$p = C \frac{1 - z^{-1}}{1 + z^{-1}} \tag{D1}$$

where z is the z-transform variable and C is a mapping constant. The p-plane transfer function was assumed to be of the form

$$G(p) = \frac{1}{1 + a_1 p + a_2 p^2 + \ldots + a_k p^k} \tag{D2}$$

Substitution of equation (D1) into equation (D2) yields an equation that becomes increasingly unwieldy as k increases. For an arbitrary k, the z-domain transfer function may be written as

$$G(z) = \frac{1 + c_1 z^{-1} + c_2 z^{-2} + \ldots + c_k z^{-k}}{b_0 + b_1 z^{-1} + b_2 z^{-2} + \ldots + b_k z^{-k}} \tag{D3}$$

The various constants in equation (D3) may be related to the constants in equations (D1) and (D2) by expansion. The resulting coefficients of digital filters are tabulated for $k = 1$ through $k = 4$ as follows:

$k = 1$

b_0	$1 + a_1 C$
b_1	$1 - a_1 C$
c_1	1

APPENDIX D

k = 2

b_o	$1 + a_1C + a_2C^2$
b_1	$2 - 2a_2C^2$
b_2	$1 - a_1C + a_2C^2$
c_1	2
c_2	1

k = 3

b_o	$1 + a_1C + a_2C^2 + a_3C^3$
b_1	$3 + a_1C - a_2C^2 - 3a_3C^3$
b_2	$3 - a_1C - a_2C^2 + 3a_3C^3$
b_3	$1 - a_1C + a_2C^2 - a_3C^3$
c_1	3
c_2	3
c_3	1

k = 4

b_o	$1 + a_1C + a_2C^2 + a_3C^3 + a_4C^4$
b_1	$4 + 2a_1C - 2a_3C^3 - 4a_4C^4$
b_2	$6 - 2a_2C^2 + 6a_4C^4$
b_3	$4 - 2a_1C + 2a_3C^3 - 4a_4C^4$
b_4	$1 - a_1C + a_2C^2 - a_3C^3 + a_4C^4$
c_1	4
c_2	6
c_3	4
c_4	1

APPENDIX D

The transfer function of equation (D3) may be readily programed on a digital computer as a numerical algorithm. Let $y(n)$ represent the sampled input to the filter, and let $y_f(n)$ represent the sampled output of the filter. The computer realization of equation (D3) reads

$$y_f(n) = \frac{1}{b_o}\Big[y(n) + c_1 y(n-1) + c_2 y(n-2) + \ldots + c_k y(n-k) - b_1 y_f(n-1) - c_2 y_f(n-2) - \ldots - c_k y_f(n-k)\Big] \tag{D4}$$

The three types of filters considered were Butterworth, Chebyshev with 3-dB ripple, and maximally flat-time delay. Detailed consideration of these filter characteristics are provided in such synthesis texts as Van Valkenburg (ref. 10) and Weinberg (ref. 11). The order of each filter was varied from $k = 1$ through $k = 4$. Actually all three filters are identical for $k = 1$. The basic low-pass p-plane normalized function for each filter was adjusted to have a reference cut-off frequency of 1 rad/sec. The cut-off frequency was defined as the highest frequency at which the response is 3 dB below the direct-current level. The coefficients of the reference low-pass analog filters used are as follows:

$k = 1$	a_1
Butterworth	1
Chebyshev (3 dB)	1
Maximally flat-time delay	1

$k = 2$	a_1	a_2
Butterworth	1.4142136	1.0000000
Chebyshev (3 dB)	0.9109423	1.4125335
Maximally flat-time delay	1.3600000	0.6165333

$k = 3$	a_1	a_2	a_3
Butterworth	2.0000000	2.0000000	1.0000000
Chebyshev (3 dB)	3.7045854	2.3832960	3.9905138
Maximally flat-time delay	1.7500000	1.2250000	0.3572917

$k = 4$	a_1	a_2	a_3	a_4
Butterworth	2.6131259	3.4142136	2.6131259	1.0000000
Chebyshev (3 dB)	2.2869936	6.6056731	3.2860053	5.6501357
Maximally flat-time delay	2.1300000	1.9443857	0.9203426	0.1960330

APPENDIX D

The constant C in equation (D1) can be determined from the required mapping correspondence between the p-plane and the s-plane. Let μ represent the p-plane imaginary axis variable and ω represent the radian frequency in the s-plane. Assume that the time between samples is t_s. It can be shown that for $\omega << 1/t_s$, ω and μ are related by

$$\mu \approx \frac{C\omega}{2} t_s \tag{D5}$$

Thus, if μ_r is some reference analog frequency and ω_r is the corresponding actual design frequency, the constant C is

$$C = \frac{2\mu_r}{\omega_r t_s} \tag{D6}$$

Accurate simulation of the digital filter was ensured by using 100 sample points during the transmitted pulsewidth t_p – that is, $t_p = 100t_s$. Let $B = \omega_r/2\pi$ where B is the bandwidth of the desired filter. With these substitutions and the assumption that $\mu_r = 1$, the constant C is given by

$$C = \frac{100}{\pi B t_p} \tag{D7}$$

REFERENCES

1. Povejsil, Donald J.; Raven, Robert S.; and Waterman, Peter: Airborne Radar. D. Van Nostrand Co., Inc., c.1961.

2. Muhleman, D. O.: Radar Scattering From Venus and the Moon. Astron. J., vol. 69, no. 1, Feb. 1964, pp. 34-41.

3. Evans, J. V.; and Pettengill, G. H.: The Scattering Behavior of the Moon at Wavelengths of 3.6, 68, and 784 Centimeters. J. Geophys. Res., vol. 68, no. 2, Jan. 15, 1963, pp. 423-447.

4. Evans, John V.: Radar Signatures of the Planets. Planetology and Space Mission Planning. Ann. N.Y. Acad. Sci., vol. 140, art. 1, Dec. 16, 1966, pp. 196-257.

5. Muhleman, Duane O.; Goldstein, Richard; and Carpenter, Roland: A Review of Radar Astronomy – Part I. IEEE Spectrum, vol. 2, no. 10, Oct. 1965, pp. 44-55; A Review of Radar Astronomy – Part II. IEEE Spectrum, vol. 2, no. 11, Nov. 1965, pp. 78-89.

6. Anon.: Surveyor III Mission Report. Tech. Rep. 32-1177 (Contract No. NAS 7-100), Jet Propulsion Lab., California Inst. Technol.
   Part I. Mission Description and Performance, Sept. 1, 1967.
   Part II. Scientific Results, June 1, 1967.

7. Skolnik, Merrill I.: Introduction to Radar Systems. McGraw-Hill Book Co., Inc., 1962.

8. Barton, David K.: Radar System Analysis. Prentice-Hall, Inc., c.1964.

9. Kaiser, J. F.: Digital Filters. System Analysis by Digital Computer, Franklin F. Kuo and James F. Kaiser, eds., John Wiley & Sons, Inc., c.1966, pp. 218-285.

10. Van Valkenburg, M. E.: Introduction to Modern Network Synthesis. John Wiley & Sons, Inc., c.1960.

11. Weinberg, Louis: Network Analysis and Synthesis. McGraw-Hill Book Co., Inc., 1962.

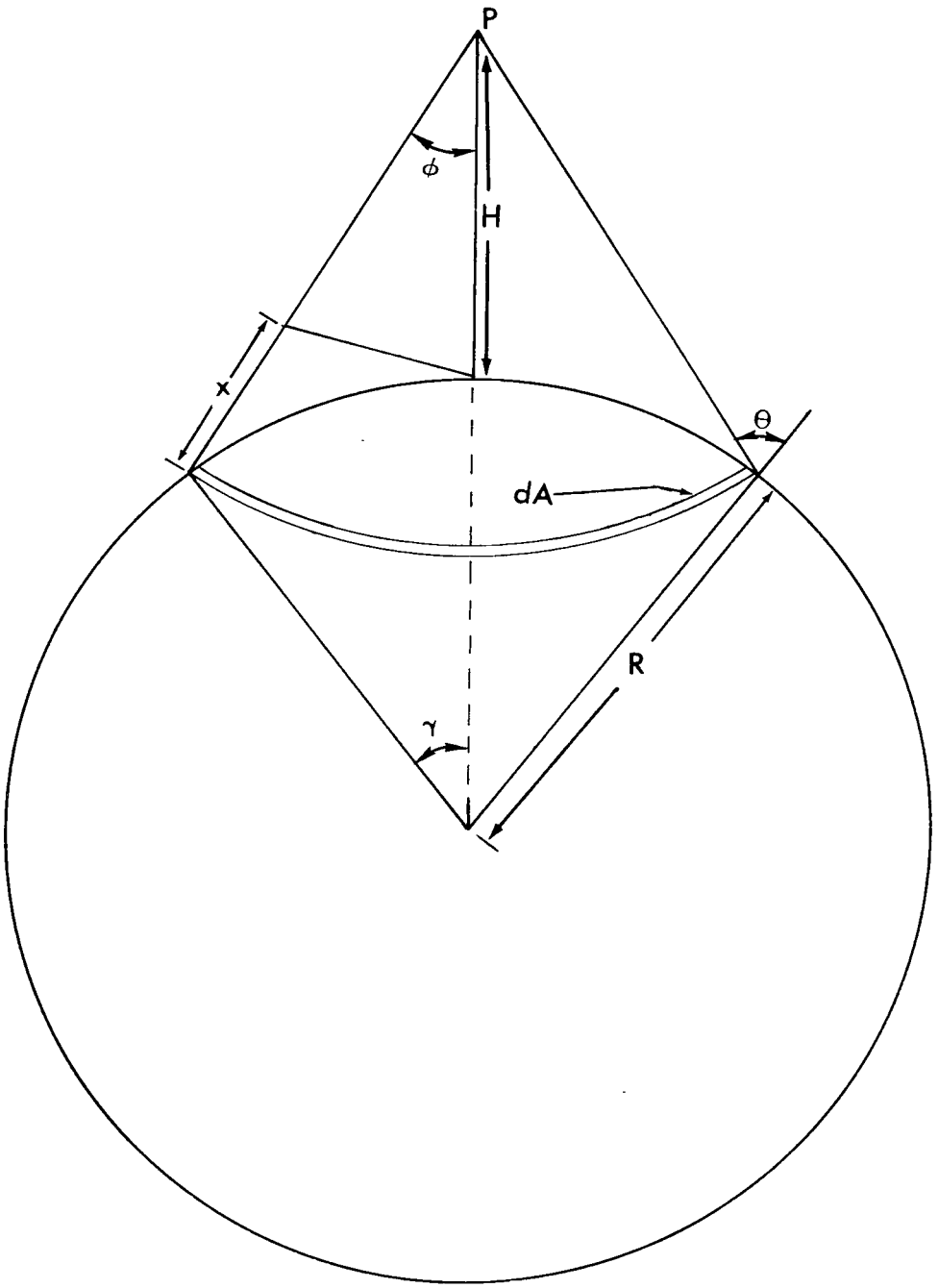

Figure 1.- Geometry of model of planetary radar altimeter.

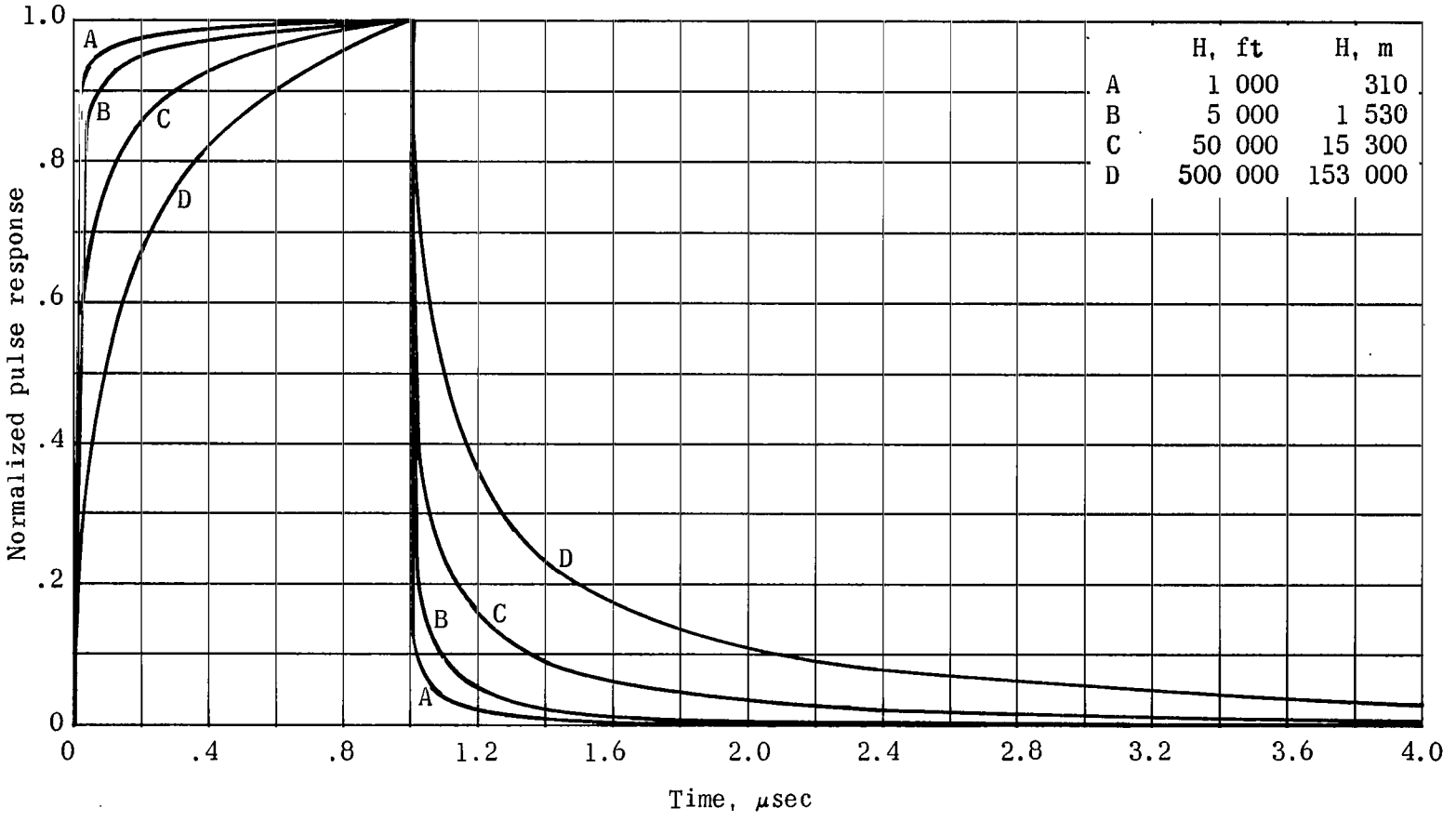

(a) $\alpha = 0.01$.

Figure 2.- Effect of radar altitude on normalized pulse response for values of Muhleman coefficient.

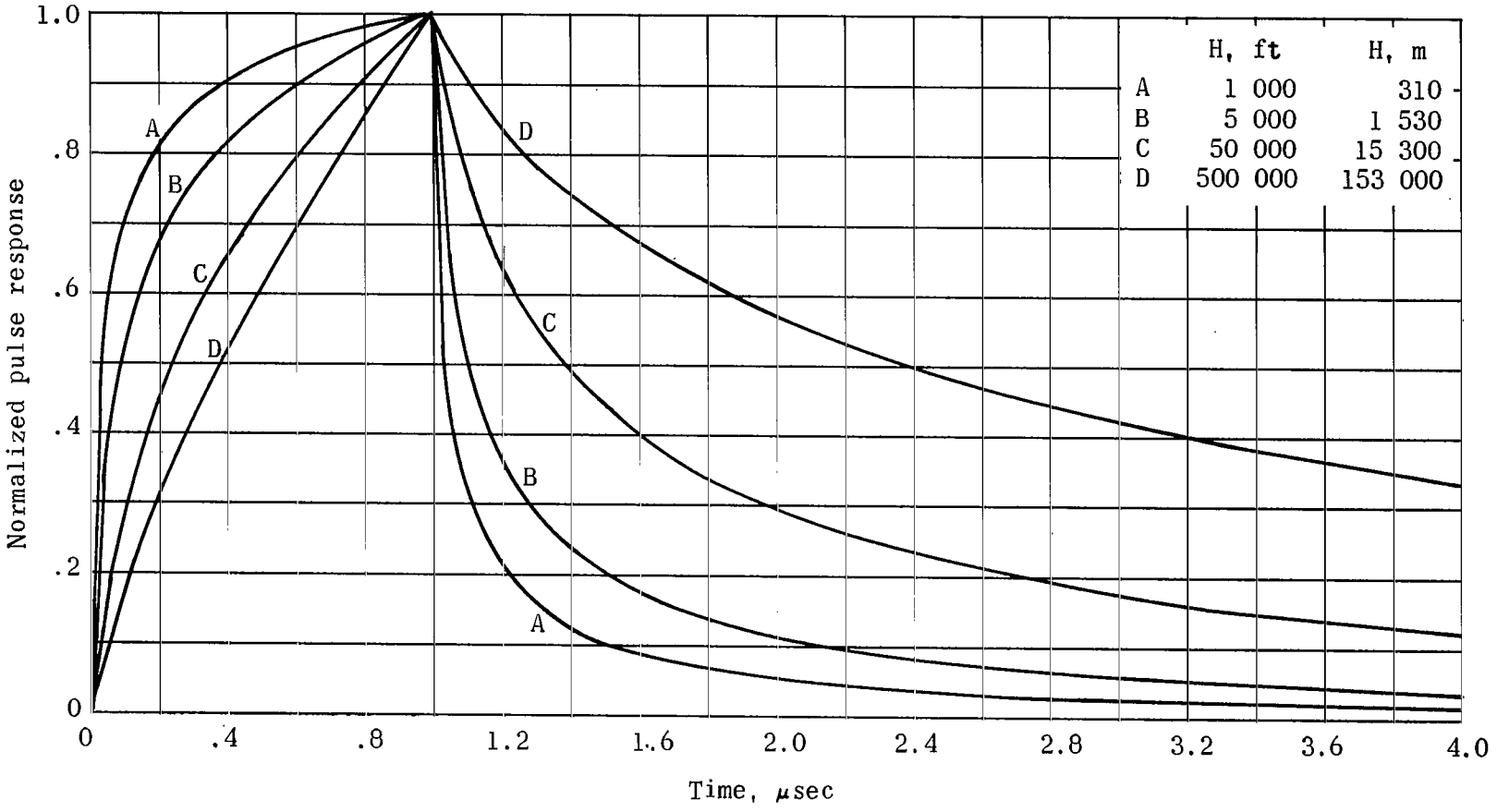

(b) $\alpha = 0.1$.

Figure 2.- Continued.

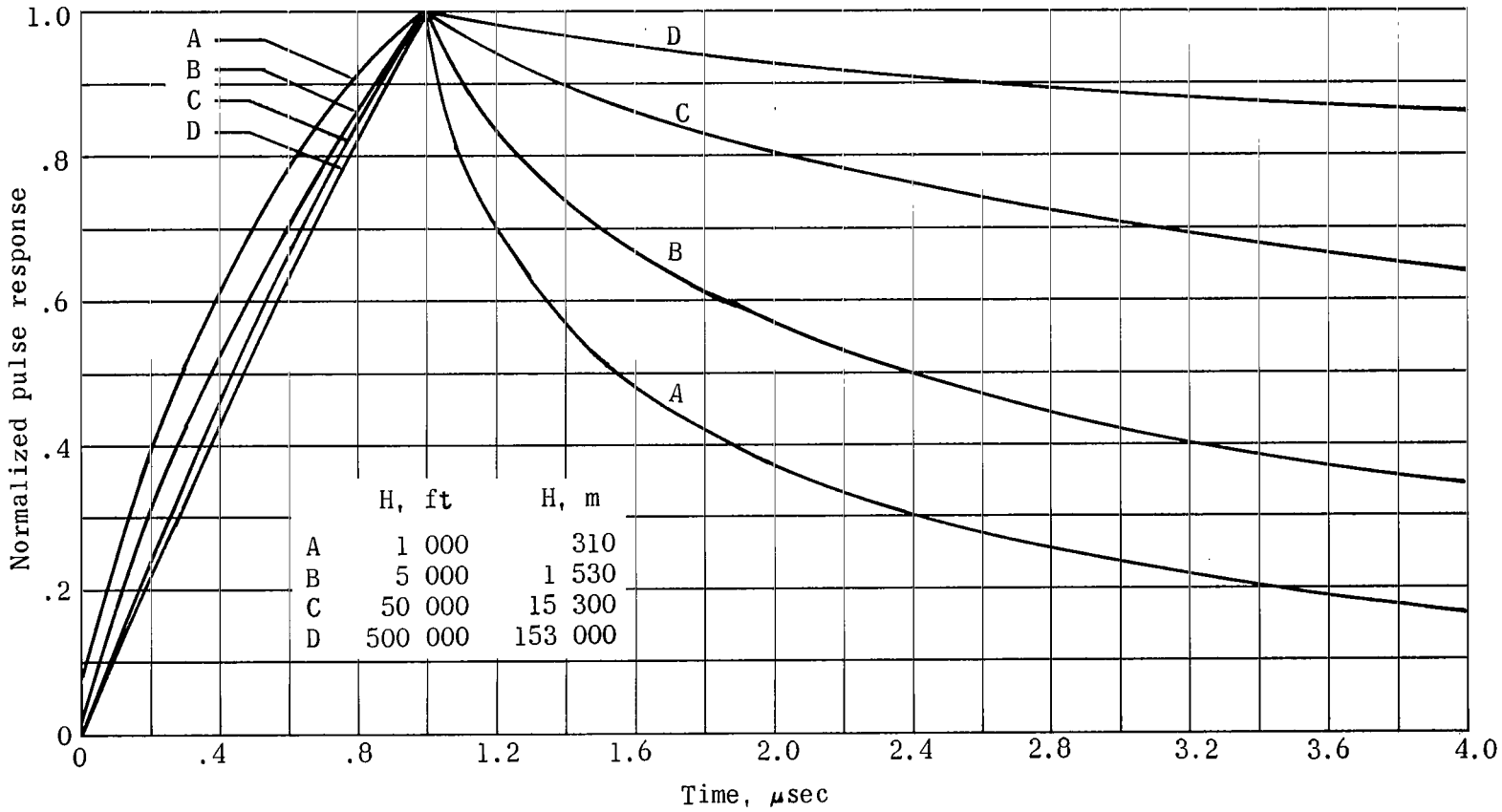

(c) $\alpha = 1.0$.

Figure 2.- Concluded.

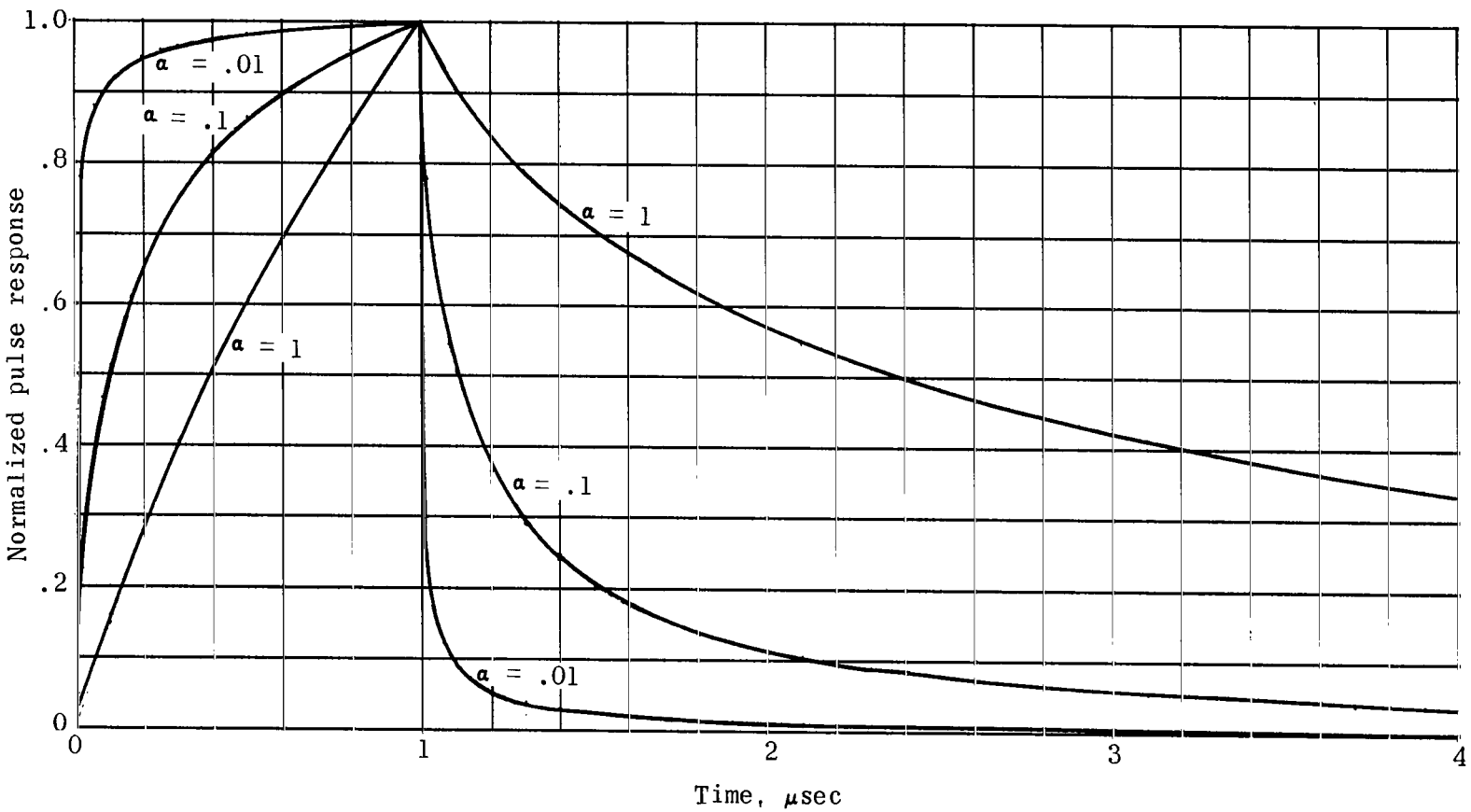

(a) H = 5000 ft (1530 m).

Figure 3.- Effect of Muhleman coefficient on normalized pulse response at various radar altitudes.

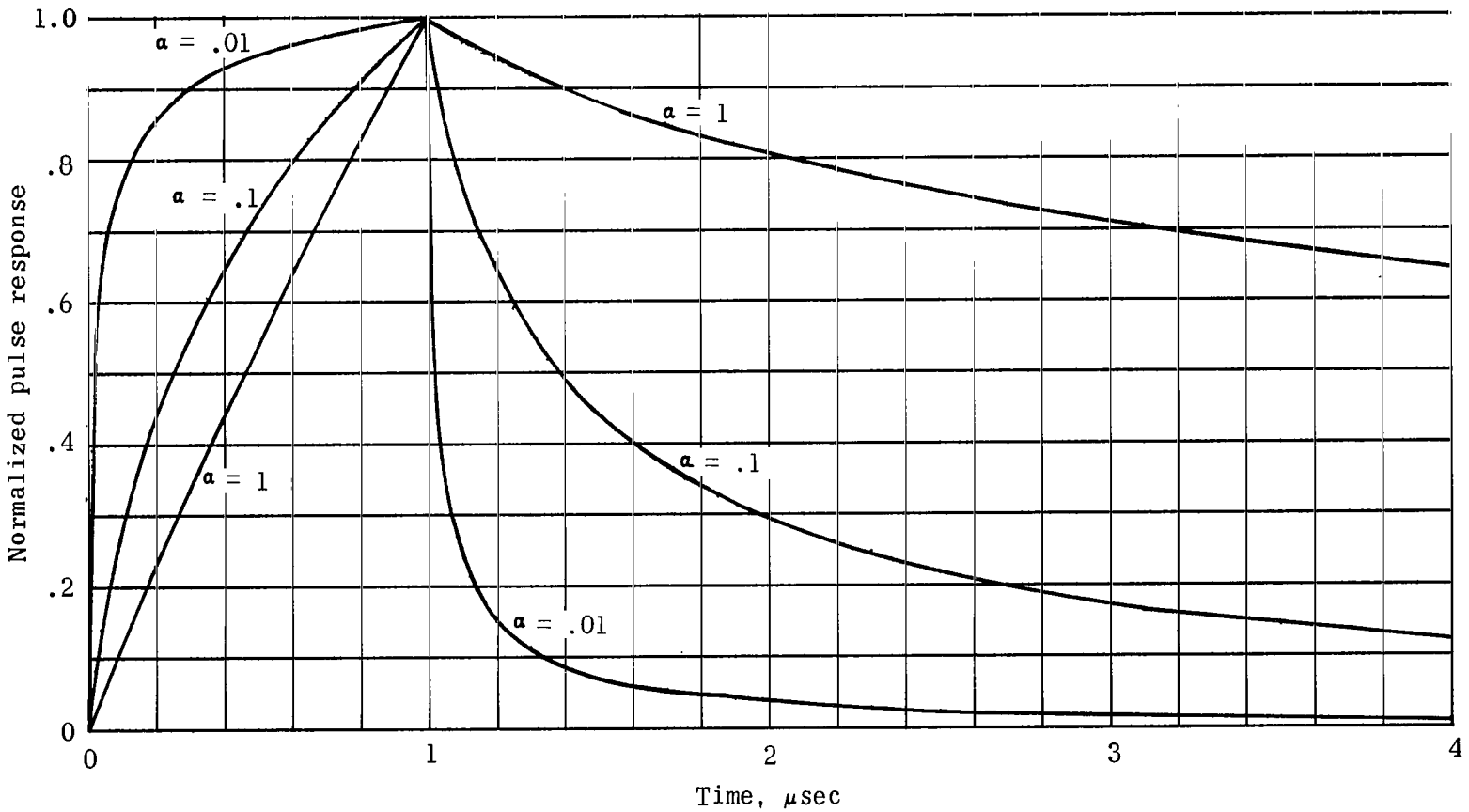

(b) H = 50 000 ft (15 300 m).

Figure 3.- Continued.

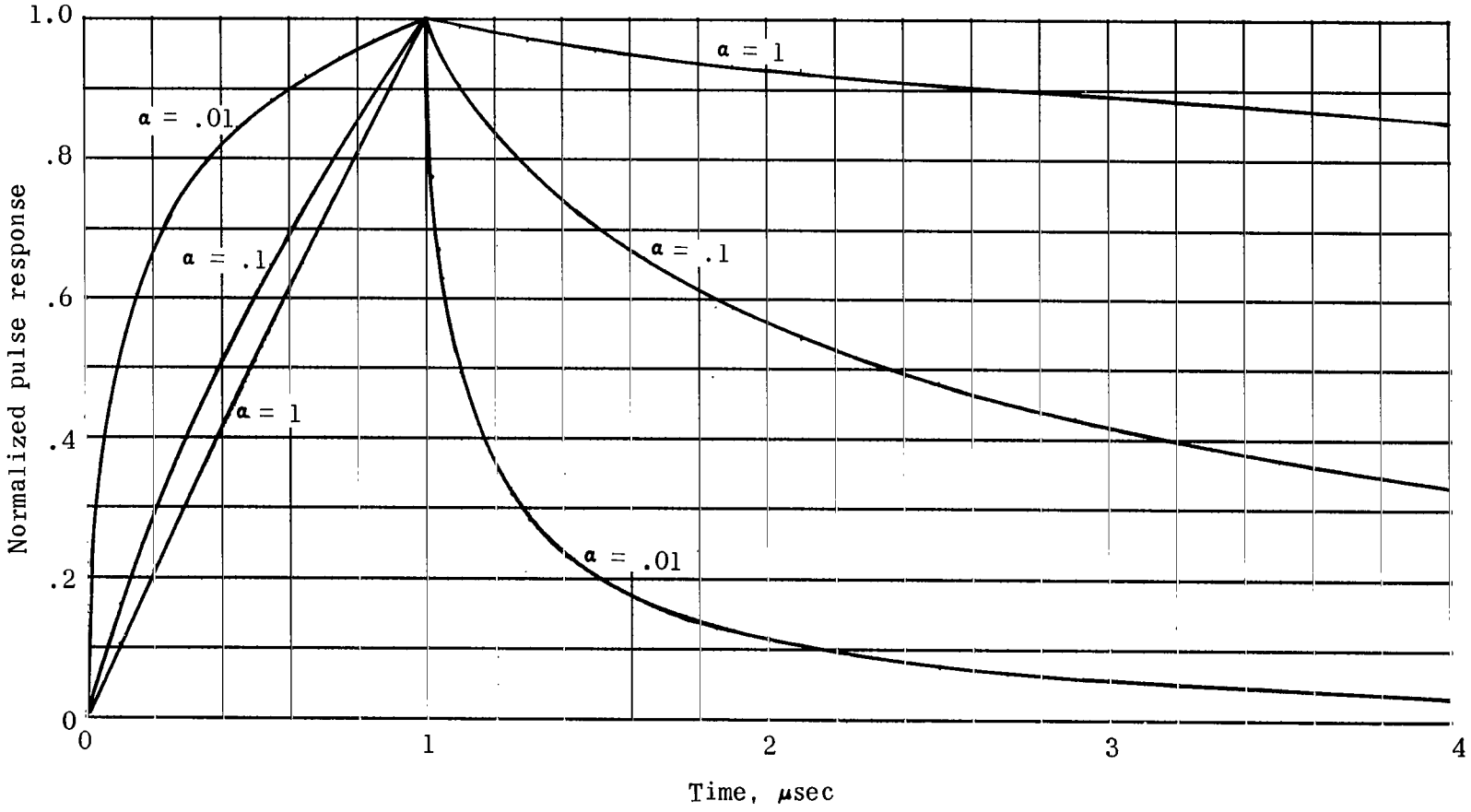

(c) H = 500 000 ft (153 000 m).

Figure 3.- Concluded.

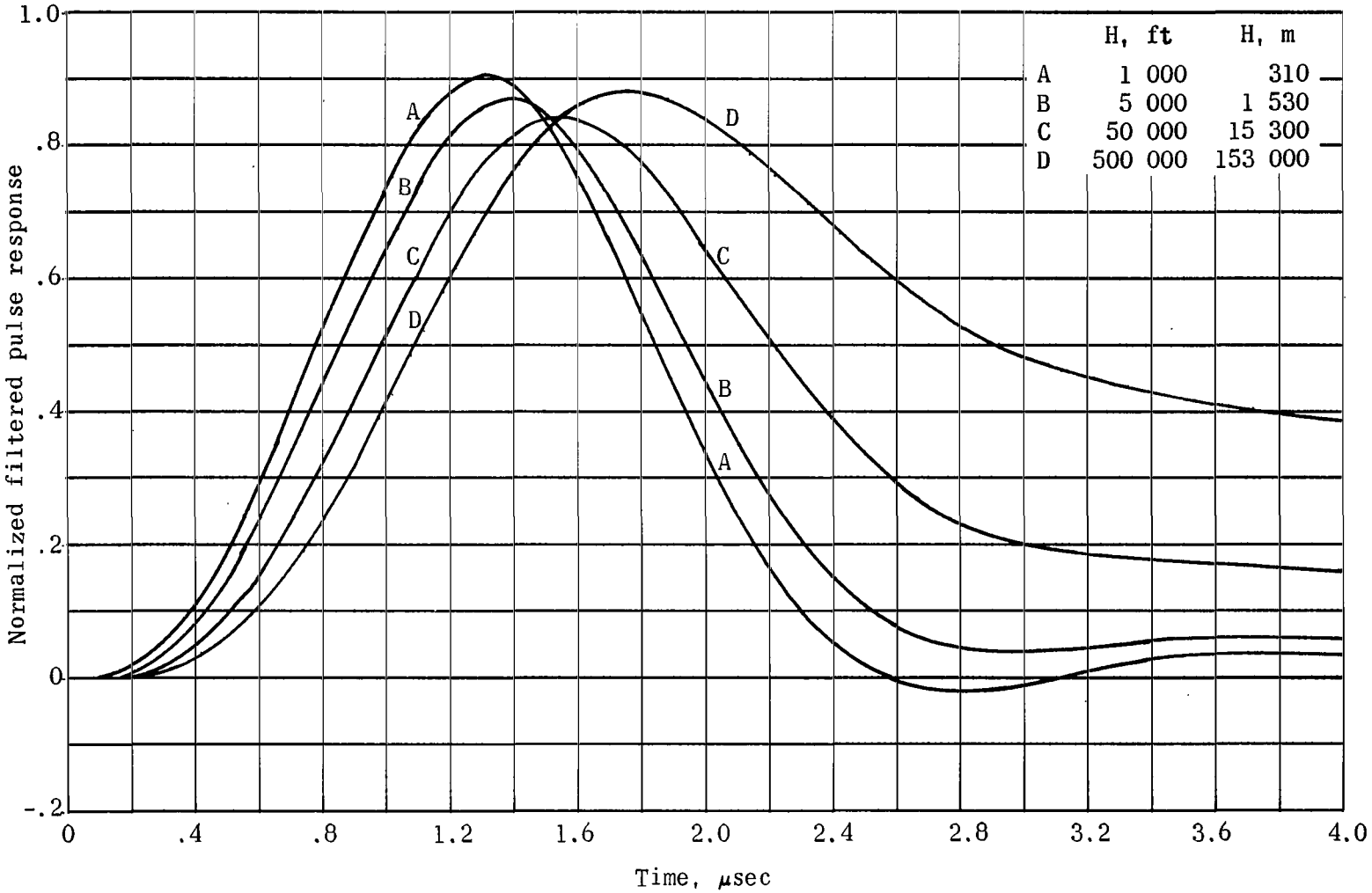

(a) Three-pole Butterworth filter.

Figure 4.- Normalized filtered pulse responses at various radar altitudes. $\alpha = 0.1$; $t_p = 1$ μsec; $B = 0.5/t_p$.

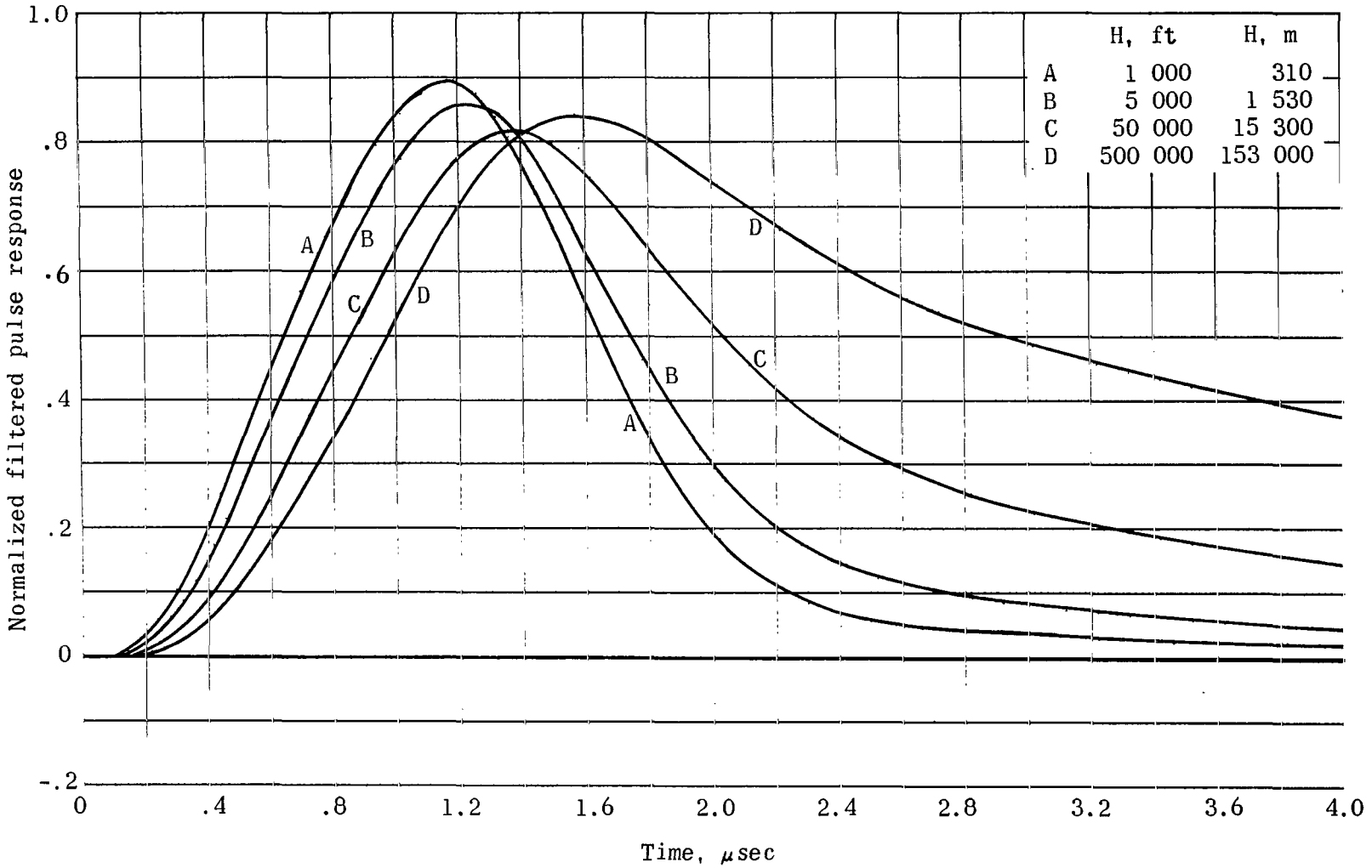

(b) Three-pole maximally flat-time-delay filter.

Figure 4.- Continued.

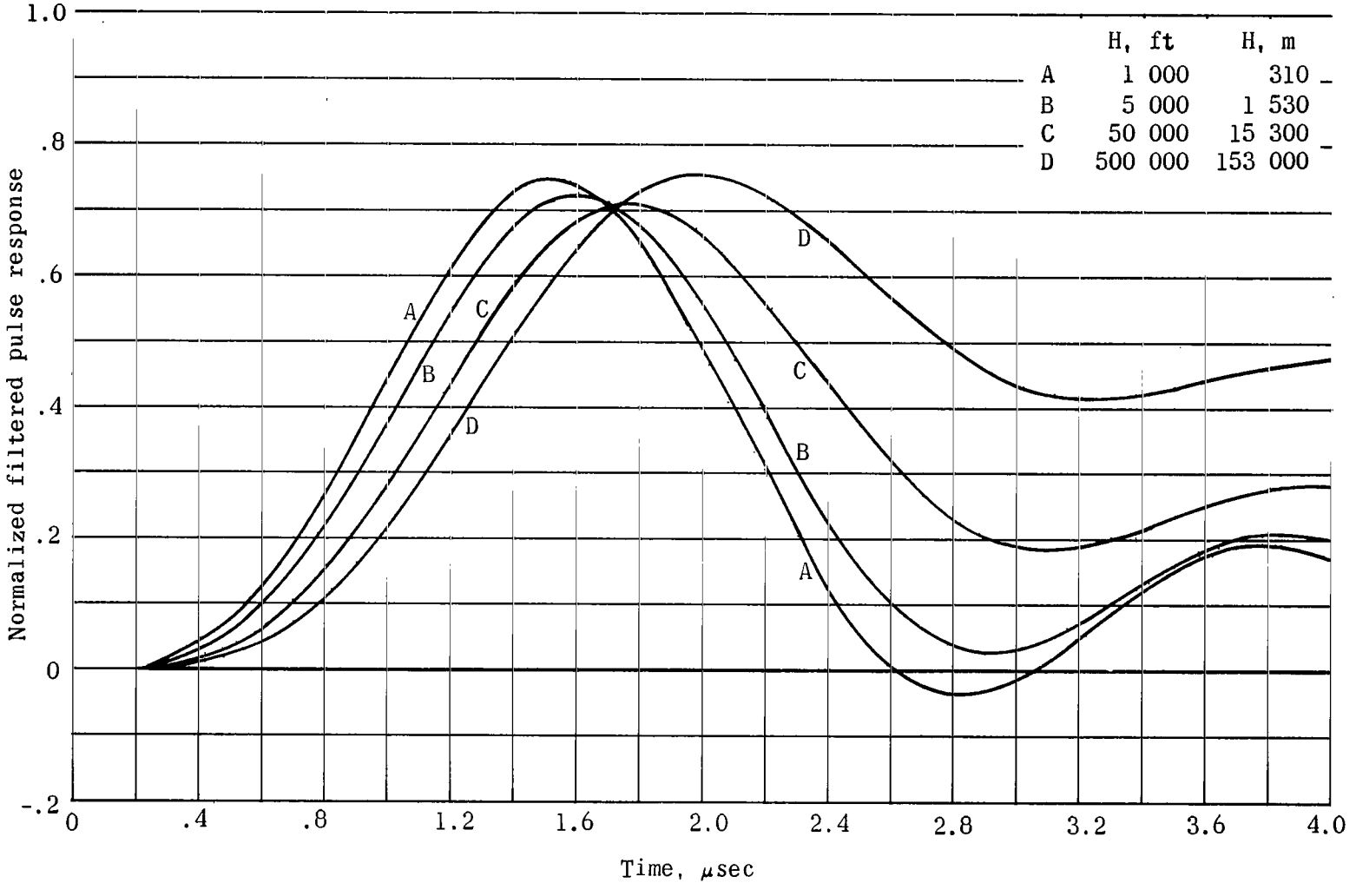

(c) Three-pole Chebyshev (3-dB ripple) filter.

Figure 4.- Concluded.

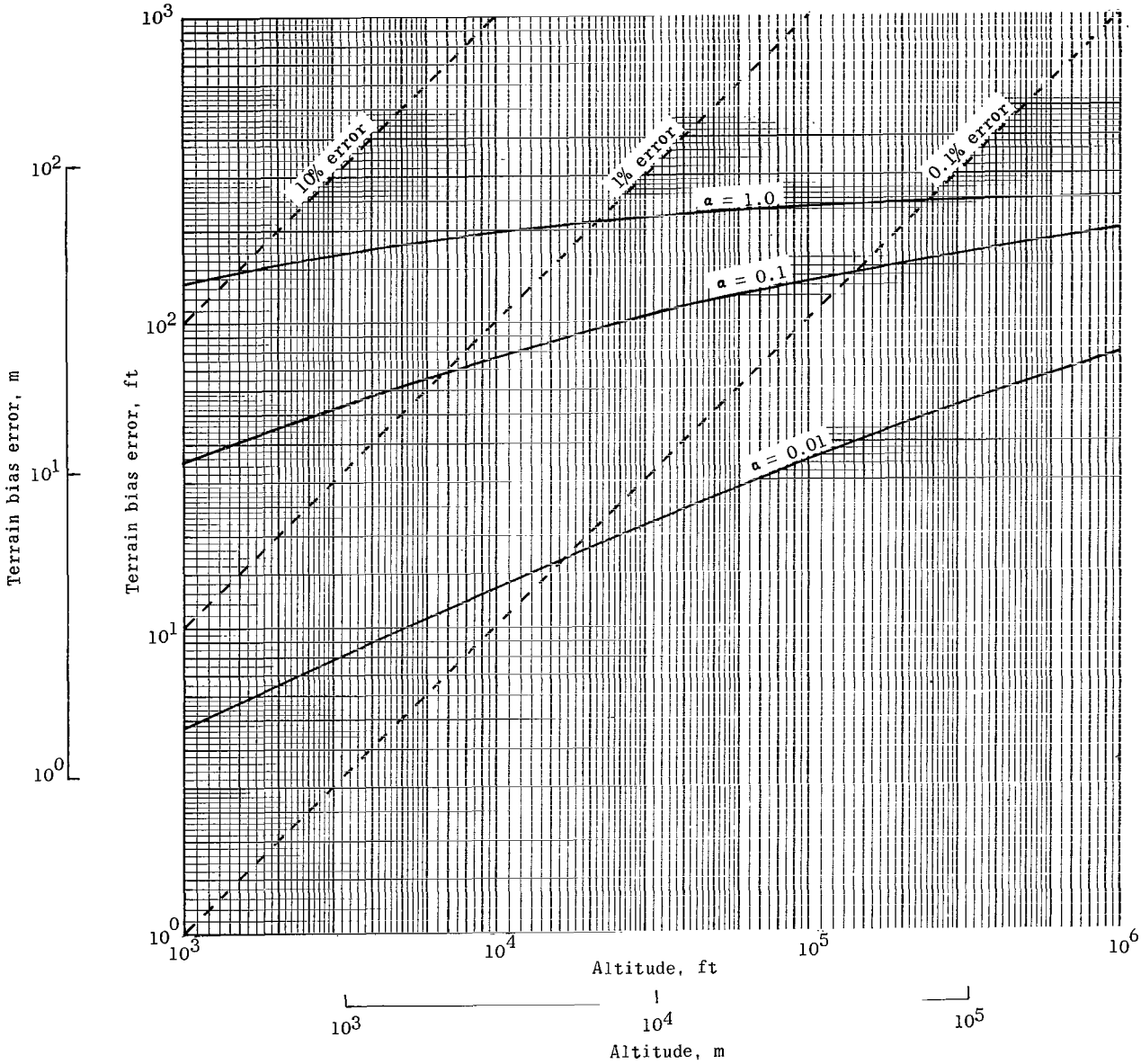

(a) Three-pole Butterworth filter.

Figure 5.- Terrain bias error as a function of altitude for various Muhleman coefficients. t_p = 1 μsec; B = 0.5/t_p.

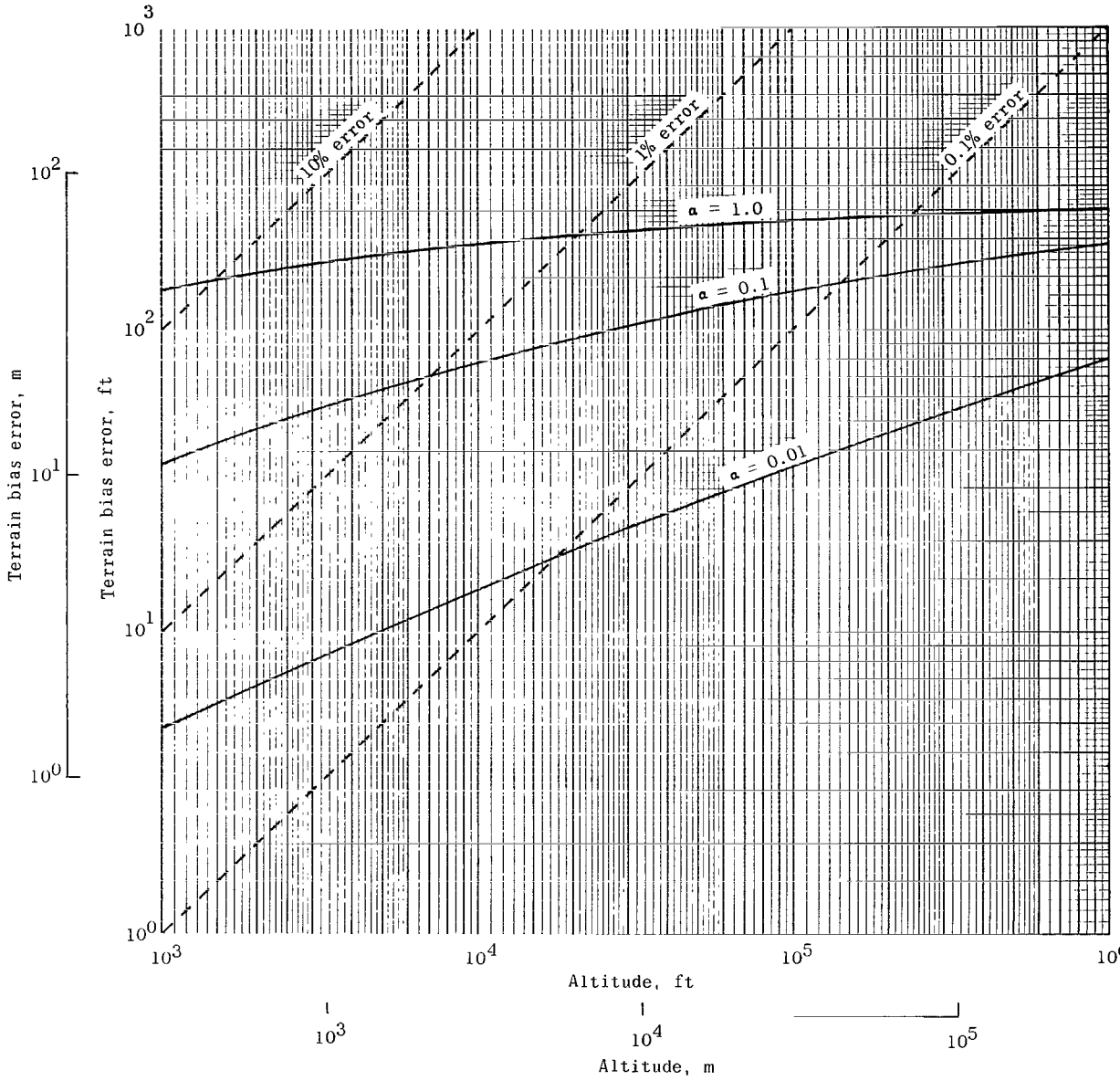

(b) Three-pole maximally flat-time-delay filter.

Figure 5.- Continued.

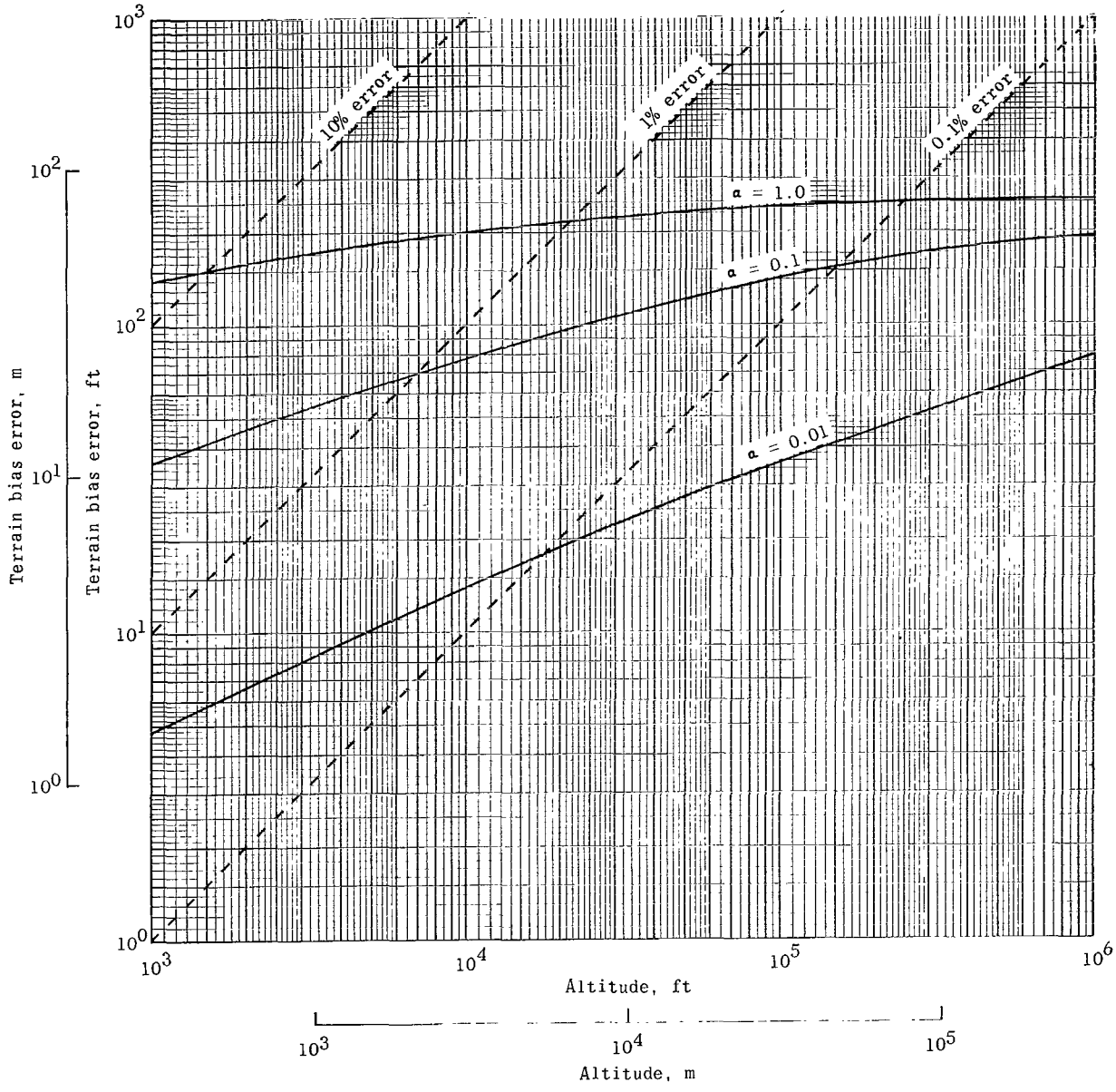

(c) Three-pole Chebyshev (3-dB ripple) filter.

Figure 5.- Concluded.

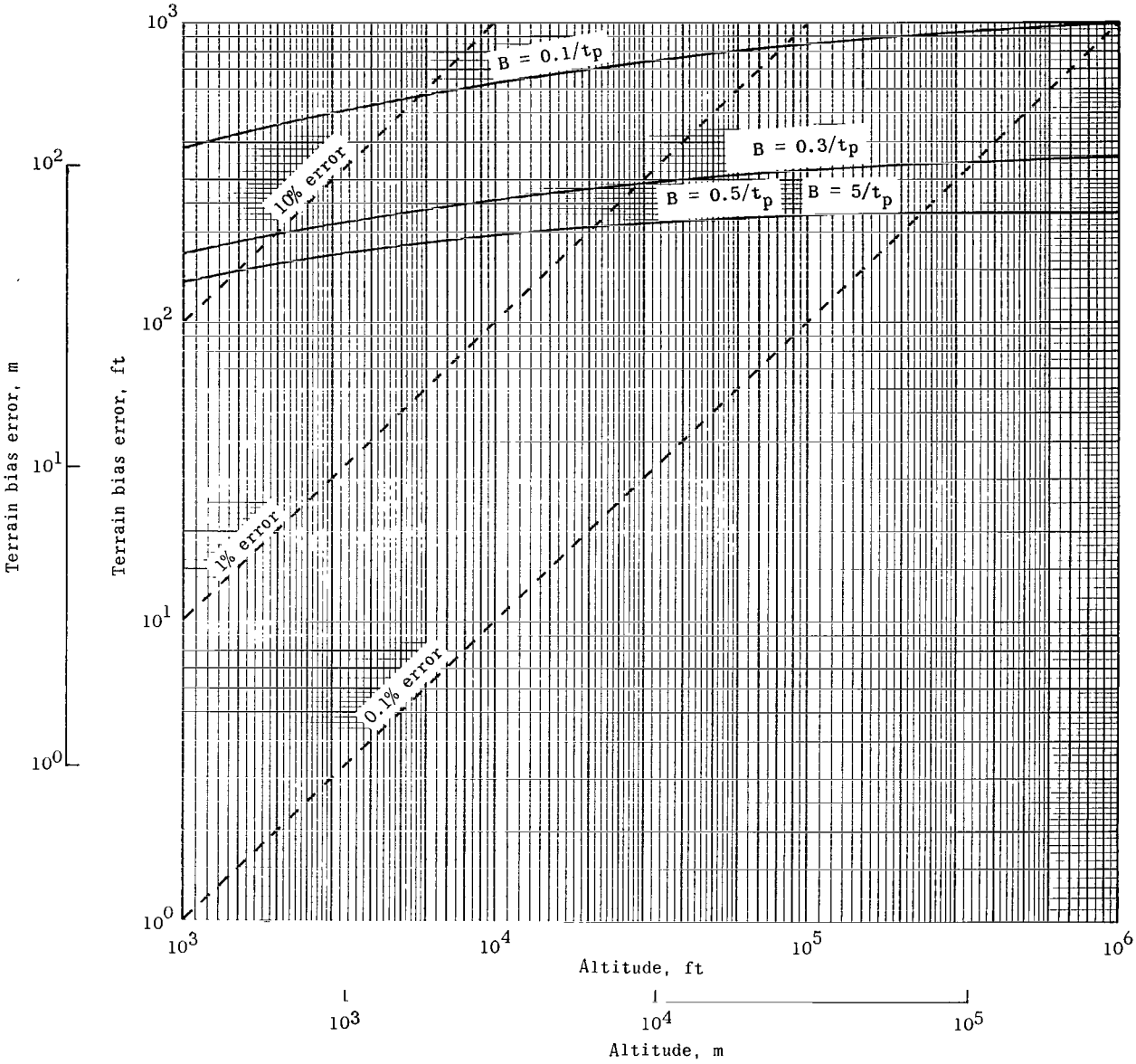

Figure 6.- Terrain bias error as a function of altitude for various bandwidths. Three-pole Butterworth filter; t_p = 1 μsec; $0.01 \leqq \alpha \leqq 1.0$.

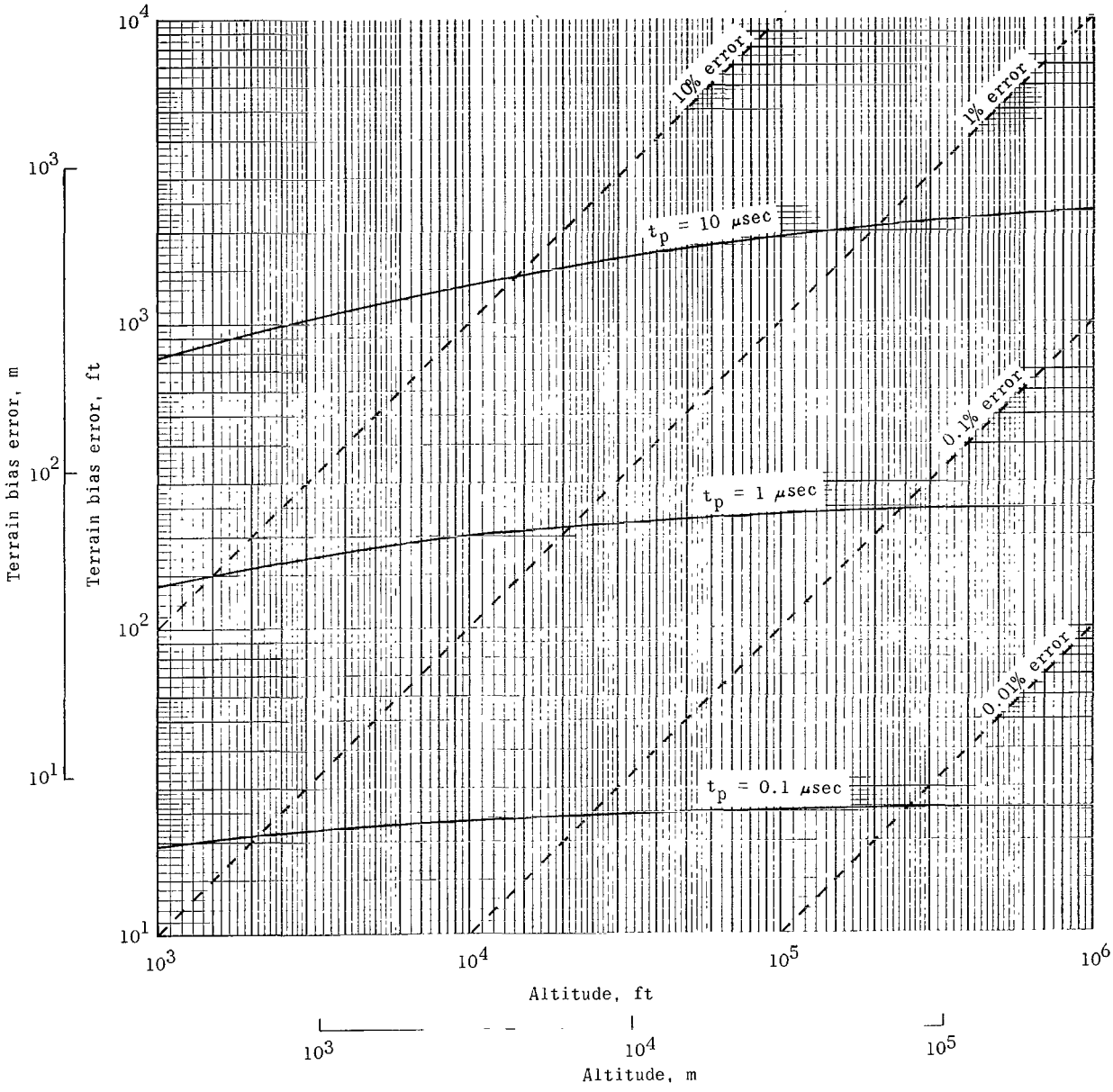

Figure 7.- Terrain bias error as a function of altitude for various pulsewidths. Three-pole Butterworth filter; $B = 0.5/t_p$; $0.01 \leqq \alpha \leqq 1.0$.

NATIONAL AERONAUTICS AND SPACE ADMINISTRATION
WASHINGTON, D. C. 20546

OFFICIAL BUSINESS

FIRST CLASS MAIL

POSTAGE AND FEES PAID
NATIONAL AERONAUTICS AN
SPACE ADMINISTRATION

POSTMASTER: If Undeliverable (Section 15
Postal Manual) Do Not Retu

"The aeronautical and space activities of the United States shall be conducted so as to contribute . . . to the expansion of human knowledge of phenomena in the atmosphere and space. The Administration shall provide for the widest practicable and appropriate dissemination of information concerning its activities and the results thereof."

—NATIONAL AERONAUTICS AND SPACE ACT OF 1958

NASA SCIENTIFIC AND TECHNICAL PUBLICATIONS

TECHNICAL REPORTS: Scientific and technical information considered important, complete, and a lasting contribution to existing knowledge.

TECHNICAL NOTES: Information less broad in scope but nevertheless of importance as a contribution to existing knowledge.

TECHNICAL MEMORANDUMS: Information receiving limited distribution because of preliminary data, security classification, or other reasons.

CONTRACTOR REPORTS: Scientific and technical information generated under a NASA contract or grant and considered an important contribution to existing knowledge.

TECHNICAL TRANSLATIONS: Information published in a foreign language considered to merit NASA distribution in English.

SPECIAL PUBLICATIONS: Information derived from or of value to NASA activities. Publications include conference proceedings, monographs, data compilations, handbooks, sourcebooks, and special bibliographies.

TECHNOLOGY UTILIZATION PUBLICATIONS: Information on technology used by NASA that may be of particular interest in commercial and other non-aerospace applications. Publications include Tech Briefs, Technology Utilization Reports and Notes, and Technology Surveys.

Details on the availability of these publications may be obtained from:

SCIENTIFIC AND TECHNICAL INFORMATION DIVISION

NATIONAL AERONAUTICS AND SPACE ADMINISTRATION

Washington, D.C. 20546